Electronic Supplementary Material (ESI) for Lab on a Chip.

Supplementary Information

Comsol simulation of the ECM with chambers

Comsol Multiphysics 5.3a is employed to compute the distribution of the von Mises stress in the ECM region via finite element method (FEM). As Fig. 2F2 shows, the ECM region is considered as linear elastomer with the 1.06 g/cm^3 density of, 300.0 Pa Young's modulus and 0.2 Poisson's ratio[1-3]. The blue surrounding region is PDMS with its 0.97 g/cm^3 density, 750.0 kPa Young's modulus and 0.49 Poisson's ratio and set as fixed constraint. Moreover, the ECM region is endued with preset stress value of 300.0 Pa and corresponding prestrain value of 1. All these preset conditions help generate stress field in the ECM region.

Simulation and experiments of the ECM with circular chambers

The ECM with circular chambers are simulated simultaneously and experimentally studied with the same conditions and parameters, as is shown in Fig. S1. The simulation indicates that the ECM outside circular chamber designs would have uniform strain field. In that case according to our experimental results, the outside chamber are distributed with homogenous collagen fibers (Fig. S1 (B)), and the metastatic breast cancer cells MDA-MB-231 inside would be hard to migrate into the ECM region across the boundary. Even though they do, the migration efficiency would be extremely low, as is shown in Fig. S1(C). It could be concluded that the square chambers have more advantages than round ones to generate the stress concentration and help form oriented collagen fibers in the composite ECM, the MDA-MB-231 cells are able to acquire strong migration within 120 hours as to test how bio-chemical gradients affect cell motility.

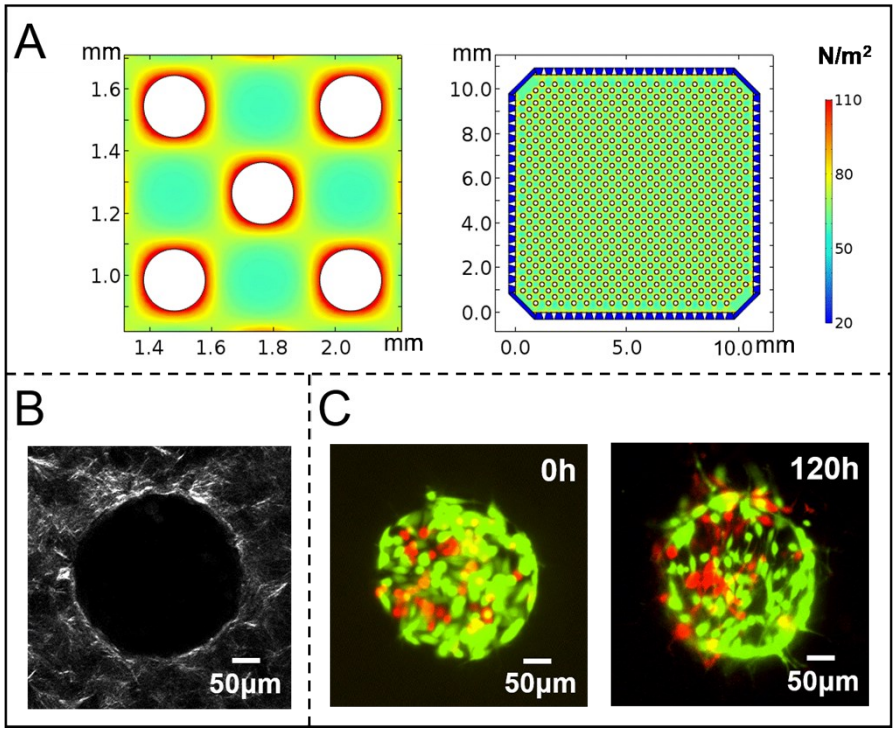

Figure S1 (A) Stress field analysis of the composite ECM with circular chambers. The uniform stress field around the circular chambers implies that oriented fibers would be barely formed and would not benefit cell migration into the ECM. (B) The distribution of collagen fibers around the circular microchamber. (C) Development of mammary epithelial cells (green) and metastatic breast cancer cells (red) in circular chamber. The migration efficiency of the metastatic breast cancer cells was extremely low.

Stability of the microchamber structures

Fig. S2 shows the amplified images showing “3×3”microchamber arrays in the microchip. At 0 h, MCF-10A-GFP cells were attached to the inner walls of ECM. Next, metastatic MDA-MB-231-RFP cells were introduced. After 120.0 h, although MDA-MB-231-RFP cells and MCF-10A-GFP cells kept proliferating and some of the cells migrated outside the chamber, the chamber structures were still clear. Therefore, it can be concluded that the microchamber structures constructed in our research are stable in space and time during the experiment.

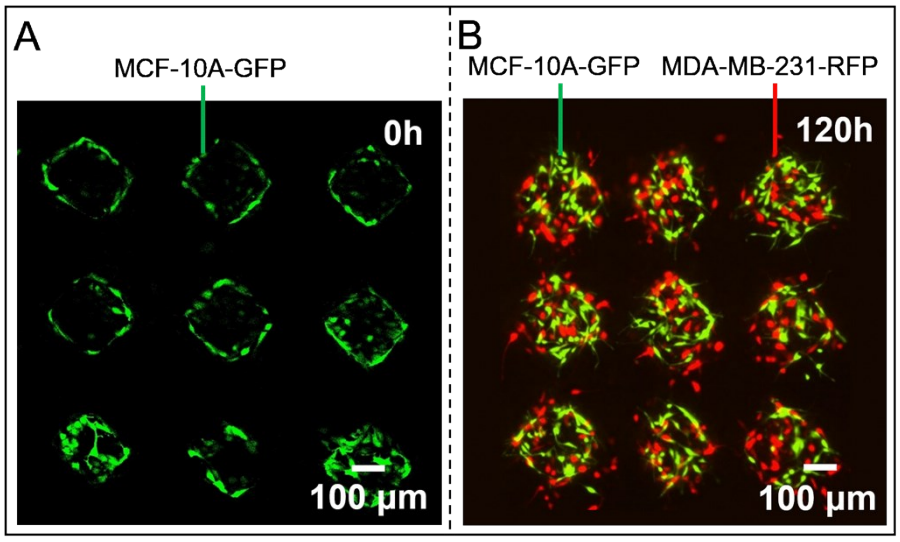

Figure S2 (A) "3×3"microchamber structures are introduced by MCF-10A-GFP cells at 0 h; (B) MDA-MB-231-RFP cells co-cultured with MCF-10A-GFP cells after 120.0 h in microchamber structures.

The test and diffusion simulation of complex gradients

Under the same experimental conditions, we repeated each gradient experiment for three times. All the gradients reached the corresponding stable states after the dyes flow into the tetragonal channels, the representative microscopic images of the gradients are shown in Fig. S3 (A1-C1). The plots in Fig. S3 (A2-C2) shows the diffusion dynamics of three biochips in time and space, where each gradient establishes gradually over time. However, it is difficult to accurately determine the time for the dye to stabilize in the gradient morphology. Since all of the dyes have good water solubility, their distribution in solutions would be in molecular forms. The molecular weights of three dyes are 1.0×10^4 Da (Rhodamine-Dextran), 3.0×10^3 Da (FITC-Dextran) and 3.0×10^3 Da (Cascade blue-Dextran) respectively. With the SEM image displayed in Fig. 2A1, the collagen-Matrigel composite ECM is porous structure and average pore size is about 3.0 μm, which is much larger than the molecules of dyes and drugs. In this case that the sizes of the molecules are much smaller than the size of porous structures, their diffusion dynamics has been shown to mainly governed by the porous microstructure (e.g., via various fiber-molecule interactions such as collision and up-take) and is less sensitive to their molecular weights. Therefore, the diffusion dynamics of these dyes obeys the homogenized diffusion equations, with an effectivity diffusivity D [4].

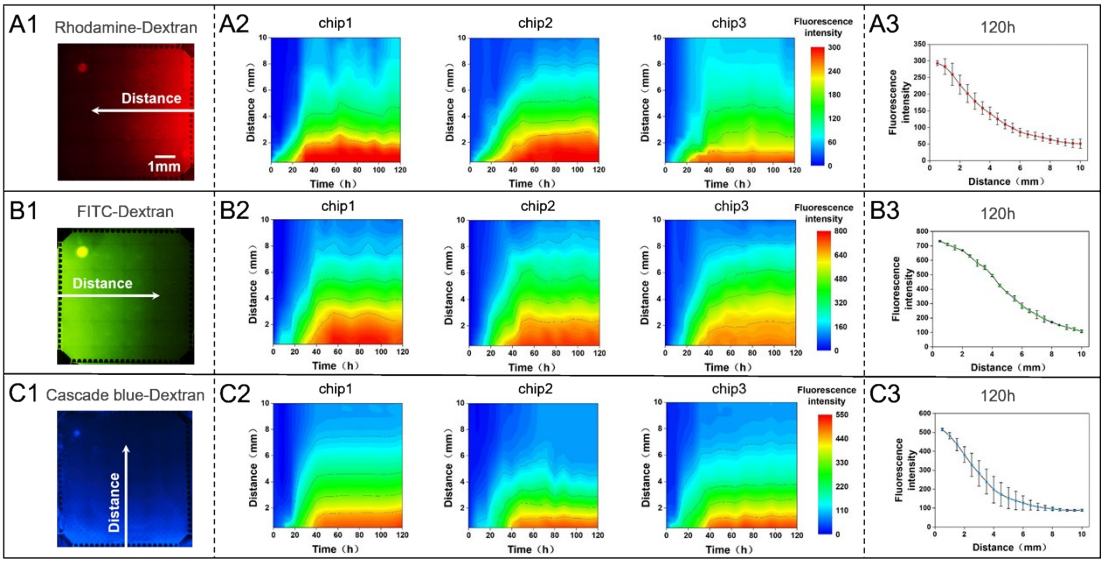

Figure S3 Dynamic establishment of the gradients. (A1-C1) The microscopic imaging of fluorescent gradients of Rhodamine-Dextran (red), FITC-Dextran (green), Cascade blue-dextran (blue). (A2-C2) Dynamic analysis of the individual gradients for three times in space and time. x axis: time. y axis: distances from the microfluidic channels. Fluorescent intensity (in arbitrary units) representing the specific concentration of the dyes. (A3-C3) The gradient analysis of the each fluorescent dye for the three chips at 120h. x axis: distances from the microfluidic channels. y axis: Fluorescent intensity (in arbitrary units).

In order to estimate the diffusivity D for each type of Dyes, we start with the following homogenized diffusion equation:

$$\frac{\partial c^{(i)}(x,t)}{\partial t} = D^{(i)}\Delta c^{(i)}(x,t) - \lambda^{(i)} c^{(i)}(x,t) \tag{1}$$

where $D^{(i)}$ is the diffusivity of Dye of type i, $\lambda^{(i)}$ is the self-degradation rate of the dye, the value of which is generally difficult to measure directly. The diffusivity can be estimated using short-time dynamics, when c(x,t) is low. In this case, the second term on the right-hand side of Eq. (1) is small and can be dropped. The corresponding solution is then given by:

$$c^{(i)}(x,t) = c_0\left[1 - erf\left(\frac{x}{\sqrt{4Dt}}\right)\right] \tag{2}$$

where erf(z) is the error function defined as

$$erf(z) = \frac{2}{\sqrt{\pi}}\int_0^z \exp(-\zeta^2)d\zeta \tag{3}$$

By fitting Eq. (2) with D as the fitting parameter to the transient data shown in Fig. R3 (i.e., for t<40 h), the diffusivity for Rhodamine-Dextran (red), FITC-Dextran (green), Cascade blue-dextran (blue) are respectively D = $1.24*10^{-7}$, $1.37*10^{-7}$, and $0.88*10^{-7}$ cm^2/s. We note that these values are consistent

with the estimates reported (10^-7 to 10^-6 cm^2/s) [5]. Since the self-degradation rates for these Dyes in our composite ECM system are unknown yet, it was unable to predict the theoretical time to reach steady state. However, it is believed that the experimental data shown in Fig. S3 are robust and informative to provide the time scale for the transition.

Comparison of the gradients with/without ECM

In order to demonstrate the unique aspect of our design, we prepared a control experiment to indicate the advantages of collagen-matrigel based ECM for long-term stable bio-chemicals. Fig. S4 presents the differences of gradient formation in our MACECM chip with ECM and without ECM. Fig. S4 (A1-A2) are the original figures from Fig. 4(B1-B2) in the manuscript, where Rhodamine-Dextran (1.0×10^4 Da, red) is utilized to examine the performance of MACECM on gradient formation. After the dye flows into the right channel, it diffuses towards the ECM region with chamber arrays and the chemical gradient is established around 40.0 h and maintained thereafter. As a comparison, the new control experiment uses the same dye at the same concentration, placed in the identical chip configuration but without gel-based ECM, as shown in Fig. S4 (B1-B2). It can be seen that once the Rhodamine-Dextran is released at the side channel, the diffusion occurs very rapidly. At the beginning, only a weak gradient forms in the distant regions from the channel (6.0 mm-10.0 mm), but after 1.0 h, the environment is homogenously colored with the dye. The result indicates that without ECM, a stable gradient is hard to be realized in MACECM chip.

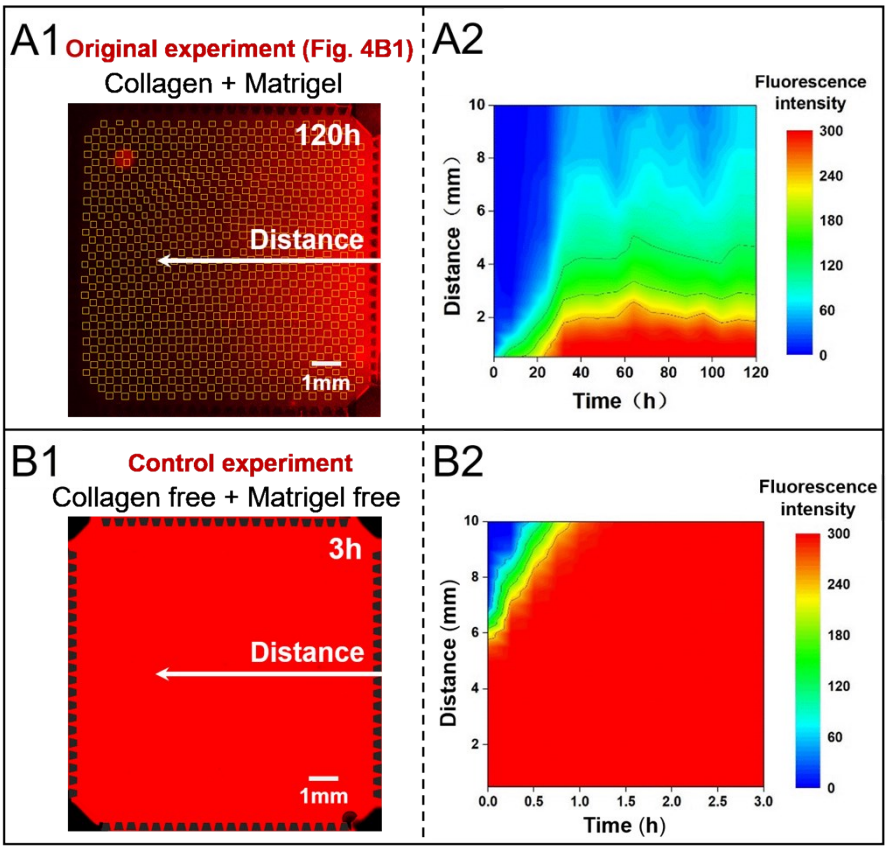

Figure S4 (A1) Rhodamine-Dextran gradient established at 120.0 h in collagen-matrigel formed ECM. The orange squares represent the 642 microchambers inside the space. (A2) The dynamic analysis of Rhodamine-Dextran gradient in time and space. x axel represents time and y axel represents the distance from the channel with fluorescent dye. The diagram indicates that the gradient formed gradually and stabilized about 40.0 h. (B1) Rhodamine-Dextran diffuse in the MACECM without ECM after 3.0 h and shows that the entire region becomes homogenous with the dye. (B2) The dynamics analysis indicates that at the beginning, some narrow region distant from the dye channel has gradient. But along with fast diffusion of dyes, the gradient vanished after 1.0 h.

Time-lapsed images of MDA-MB-231-RFP and MCF-10A-GFP co-culture in the ECM region of composite chemical gradients

Fig. S5 demonstrates the original data images of MDA-MB-231-RFP cells (red) and MCF-10A-GFP cells (green) co-cultured in the ECM region of composite chemical gradients at 0 h, 24.0 h, 48.0 h, 72.0 h, 96.0 h and 120.0 h in combined fluorescent images and respective red and green ones.

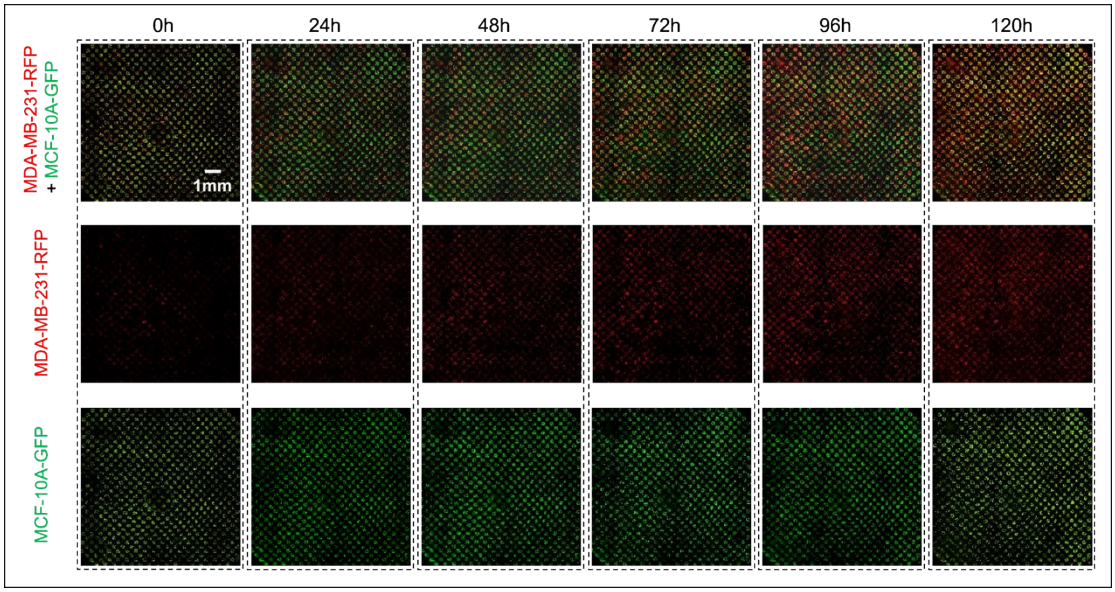

Figure S5 The fluorescent images of MDA-MB-231-RFP cells and MCF-10A-GFP cells in the ECM applied by the composite gradient, taken at every 24.0 h.

Computational model

To complement our experimental studies, we develop a computational model for the spatial-temporal evolution of the cell population in the micro-chip, which are determined by various inhibitors and growth factors diffusing in the micro-chambers. Our model is based on continuous diffusion equations for the inhibitors and growth factors, which are coupled with equations governing cell population dynamics.

In particular, the dynamics of the concentration $c^{(i)}(\mathbf{x},t)$ of chemical species *i* (which can represent EGF, DDR1 inhibitors, or MMP inhibitors) is governed by the following equation:

$$\frac{\partial c^{(i)}(\mathbf{x},t)}{\partial t} = D^{(i)}\Delta c^{(i)}(\mathbf{x},t) - \lambda^{(i)}c^{(i)}(\mathbf{x},t) - \sum_j \gamma_j \rho_j(\mathbf{x},t) \qquad (1)$$

where $D^{(i)}$ is the diffusivity, $\lambda^{(i)}$ is the self-degradation rate of the chemicals, γ_j is the up-take rate by cells of type *j* (which can represent either MDA-MB-231-RFP cells or MCF-10A-GFP cells), and ρ_j is the local cell number density. In our subsequent numerical simulations, we consider that the chemical concentrations within a micro-chamber are homogeneous (i.e., take constant values for any fixed time point *t*), which are varying from one micro-chamber to another in the micro-chip. The local cell number densities are also defined for each micro-chamber. Therefore, the numerical discretization is taken to

be consistent with the distribution of the micro-chambers on a checker-boarder lattice, i.e., each grid point in the numerical discretization represents a micro-chamber in the chip, on which the chemical concentrations and cell densities are uniquely defined.

The population dynamics of the MDA-MB-231-RFP cells in the micro-chamber at location **x** is described by

$$\frac{\partial \rho_\alpha(\mathbf{x},t)}{\partial t} = \chi_1(c^{EGF})\rho_\alpha(\mathbf{x},t)\left[1-\chi_2(c^{MMP},c^{DDR1})\rho_\alpha(\mathbf{x},t)-\rho_\beta(\mathbf{x},t)\right] \quad (2)$$

where ρ_α and ρ_β are respectively the normalized local density of MDA-MB-231-RFP cells and MCF-10A-GFP cells; χ_1 is the growth rate of MDA-MB-231-RFP cells, which depends on the concentration of EGF; χ_2 is an effective migration factor depending on the inhibitor concentrations. We note that based on the experiments, we consider the cells are mainly localized in or near their original micro-chamber where the cells were cultured and no significant long-distance migration occurred. Therefore, we do not include a diffusion term in Eq. (2) accounting for long-range cell migration. We also note that the first term ($\sim\chi_1\rho_\alpha$) on the R. H. S. of Eq. (2) dominates the initial proliferation of the MDA-MB-231-RFP cells, which is eventually suppressed by the limited space in the micro-chamber and the competition from MCF-10A-GFP cells. Such constraints and competition can be relaxed due to the migratory capability of the MDA-MD-231-RFP cells, which is quantified by the factor χ_2. For $0<\chi_2<1$, the MDA-MD-231-RFP exhibit migratory phenotypes and can break the micro-chamber and migrate into the surrounding ECM regions, leading to $\rho_\alpha>1$. For $\chi_2\geq 1$ (due to the inhibitors), the migratory phenotypes are suppressed and the cells can only proliferate within the micro-chamber, i.e., $0<\rho_\alpha<1$ and $0<\rho_\beta<1$.

Following the same reasoning, the population dynamics of the MCF-10A-GFP cells in the micro-chamber at location **x** is described by

$$\frac{\partial \rho_\beta(\mathbf{x},t)}{\partial t} = \chi_3(c^{EGF})\rho_\beta(\mathbf{x},t)\left[1-\chi_2(c^{MMP},c^{DDR1})\rho_\alpha(\mathbf{x},t)-\rho_\beta(\mathbf{x},t)\right] \quad (3)$$

where χ_3 is the growth rate of MCF-10A-GFP cells, which depends on the concentration of EGF. Based on the aforementioned analysis and our experimental results, we employ the following forms for the model parameters:

$$\chi_1(\mathbf{x},t)=1.25\cdot c^{EGF}(\mathbf{x},t),\ \chi_2(\mathbf{x},t)=0.5+c^{MMP}(\mathbf{x},t)\cdot c^{DDR1}(\mathbf{x},t),\ \chi_3(\mathbf{x},t)=c^{EGF}(\mathbf{x},t) \quad (4)$$

We would like to emphasize that the choice of these parameters are rather ad hoc, assuming

simple linear relations. Nonetheless, as shown above, our simple models can capture the key physics of the spatial-temporal evolution of the cell populations and complement our experimental studies.

Eqs. (1)-(4) are numerically solved to obtain (quasi-) steady-state distribution of cell population in the micro-chambers, which are determined by the equilibrium concentrations of various inhibitors and growth factors. We also carried out a linear sensitivity analysis which indicates that the steady-state distributions of the cell population do not sensitively depend on the choice of model parameters.

Reference

1. W. Han, S. Chen, W. Yuan, Q. Fan, J. Tian, X. Wang, L. Chen, X. Zhang, W. Wei, R. Liu, J. Qu, Y. Jiao, R. H. Austin and L. Liu, *Proceedings of the National Academy of Sciences of the United States of America*, 2016, **113**, 11208-11213.
2. N. Gjorevski and C. M. Nelson, *Integrative Biology*, 2010, **2**, 424-434.
3. E. Boghaert, J. P. Gleghorn, K. Lee, N. Gjorevski, D. C. Radisky and C. M. Nelson, *Proceedings of the National Academy of Sciences of the United States of America*, 2012, **109**, 19632-19637.
4. Y. Jiao and S. Torquato, Physical Biology, 2012, 9, 036009.
5. Y. Du, M. J. Hancock, J. He, J. L. Villa-Uribe, B. Wang, D. M. Cropek and A. Khademhosseini, Biomaterials, 2010, 31, 2686-2694.